**Proceedings of DETC'02**
**ASME 2002 Design Engineering Technical Conferences**
**and Computers and Information in Engineering Conference**
**Montreal, Canada, September 29 – October 2, 2002**

# DETC2002/MECH-34257

## GEOMETRIC ALGORITHMS FOR THE COMPUTATION OF THE CONSTANT-ORIENTATION WORKSPACE AND SINGULARITY SURFACES OF A SPECIAL 6-RUS PARALLEL MANIPULATOR

**Ilian A. Bonev and Clément M. Gosselin**
Département de Génie Mécanique
Université Laval
Québec, Québec, Canada G1K 7P4
e-mail: gosselin@gmc.ulaval.ca

### ABSTRACT

This paper studies the kinematic geometry of a special 6-*RUS* parallel manipulator for which the axes of all base actuated *R*-joints coincide, the centers of all *U*-joints move along the same circular track, and the platform *S*-joints coincide in pairs. Particularly, the paper presents a geometric algorithm for the computation of the constant-orientation workspace. An already known methodology has been enhanced to include the physical constraint, modelled as three Bohemian dome surfaces, on the *U*-joint interference. In addition, the singularity loci for a constant orientation are shown to form a quartic surface. The workspace boundaries and the singularity loci are analytically computed and represented as horizontal cross-sections. Important observations are made on the singularities of general parallel mechanisms with pair-wise coincident *S*-joints. The paper also introduces the phenomenon that the workspace of some parallel mechanisms is divided into regions corresponding to different branch sets.

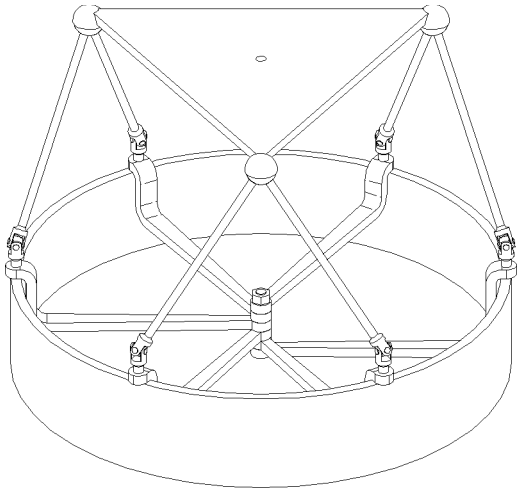

**Fig. 1 CAD Model of the Rotobot™.**

### 1 INTRODUCTION

One of the main disadvantages of parallel manipulators (PMs) is their limited and complex workspace. Thus, the size and shape of the workspace has become two of the main design criteria. As the *complete workspace* of a 6-DOF PM is a six-dimensional entity which is impossible to visualize, algorithms for various subsets of it have been proposed. One of the most popular subsets is the *constant-orientation workspace* which is the three-dimensional volume that can be attained by a point of the mobile platform when the platform is kept at a constant orientation.

The most intuitive and accurate methods of analyzing and optimizing a given design are based on a geometrical approach. A geometrical method for computing the constant-orientation workspace of a Stewart-Gough platform was first proposed by Gosselin (1990) and then revised by Merlet (1994). A detailed literature review was recently presented in (Bonev and Gosselin, 2000) where the focus was on general 6-*RUS* PMs. In this notation, *R* stands for a base actuated revolute joint, *U* for a passive universal joint, and *S* for a passive platform spherical joint.

Inspired by the same philosophy, we present in this paper a detailed geometrical study of a special 6-*RUS* PM, patented (Chi, 1999) and commercialized by Hexel Corporation (`http://www.hexel.com`) under the name *Rotobot*™ (Fig. 1). Unlike previous woks, however, our study includes not only a workspace but also a singularity analysis due to the inherent relationship between those two.

### 1.1 Notation and Description of the Architecture

Following the notation used in (Bonev and Gosselin, 2000), we denote the centers of the *U*-joints by $A_i$ and the centers of the spherical joints attached at the mobile platform by $B_i$ (in this paper $i = 1, \ldots, 6$). All points $A_i$ move along the same circular trajectory referred to as *the track* whose center is denoted by $O$. The centers of the spherical joints are pairwise coincident, i.e., $B_1 \equiv B_2$, $B_3 \equiv B_4$, and $B_5 \equiv B_6$. These centers form an equilateral triangle and lie on a circle of radius $r_B$ and center $C$.

In this paper, we will use the term *adjacent* to refer to any two chains that have a common spherical joint center. The same term will be applied to any of the corresponding elements of such two chains (e.g., points $A_1$ and $A_2$ are adjacent).

Further on, we will refer to the link connecting points $O$ and $A_i$ as *proximal link* $i$ and to the link connecting points $A_i$ and $B_i$ as *distal link* $i$. The lengths of all proximal links are equal and denoted by $r_A$. The lengths of all distal links are also equal and denoted by $\ell$. We select a fixed reference frame, called the *base frame*, with origin at $O$ and axes $x$, $y$, and $z$, such that $z$ is also the axis of all *R*-joints and the track lies in the $xy$ plane. We also select a *mobile frame* that is fixed to the mobile platform, with center $C$ and axes $x'$, $y'$, and $z'$, such that all points $B_i$ are in the $x'y'$ plane and the $x'$-axis is parallel to $B_1B_3$ (Fig. 2).

Let us denote the angle between the $x$-axis and line $OA_i$ by $\theta_i$. This angle is called *articular coordinate* $i$ and is controlled by the motor at revolute joint $i$. The mobile platform's position with respect to the base frame is defined by vector $\mathbf{c}$, along line $OC$, while the platform orientation is described by a rotation matrix $\mathbf{R}$ that is defined by three Euler angles. The three coordinates of point $C$ and the three Euler angles constitute the so-called *generalized coordinates*. The latter define completely the *pose* (the position and orientation) of the mobile platform.

Finally, we will add the superscript $'$ to a vector when the latter is expressed in the mobile frame. No superscript will mean that the vector is expressed in the base frame. Thus, the vectors, expressed in the base frame, along lines $OA_i$, $OB_i$, and $CB_i$ are respectively denoted by $\mathbf{a}_i$, $\mathbf{b}_i$, and $\mathbf{m}_i$.

### 1.2 Inverse Kinematics

The task of computing the set of articular coordinates from the set of generalized coordinates is referred to as the *inverse kinematic problem* (IKP). The solution to this problem for the general 6-*RUS* PM was described in (Bonev and Gosselin, 2000). Herein, we provide the simplified procedure for the *Rotobot*.

Geometrically, for each serial chain, the problem can be regarded as the one of finding the intersection point(s) between a sphere, of radius $\ell$ and center $B_i$, and the track circle. Clearly, this problem may have an infinite number of real solutions, two solutions, a single one, or none at all.

Let the unit vector along distal link $i$ be denoted by $\mathbf{n}_i$:

$$\ell \mathbf{n}_i = \mathbf{c} + \mathbf{R}\mathbf{m}'_i - \mathbf{a}_i. \tag{1}$$

Squaring both sides of Eq. 1 gives us

$$\ell^2 = (\mathbf{c} + \mathbf{R}\mathbf{m}'_i - \mathbf{a}_i)^T(\mathbf{c} + \mathbf{R}\mathbf{m}'_i - \mathbf{a}_i), \tag{2}$$

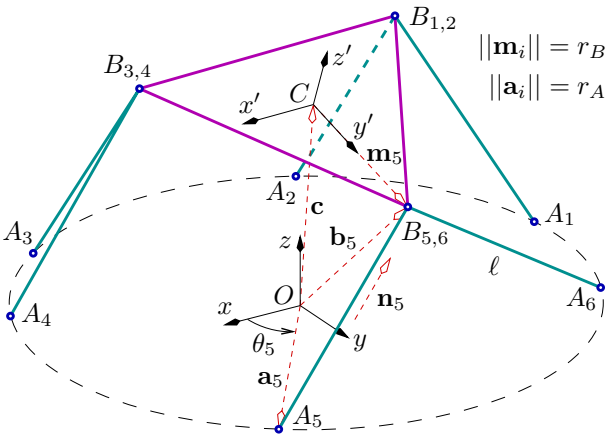


**Fig. 2 Schematic and notation of the Rotobot**

$$\ell^2 = \|\mathbf{b}_i\|^2 + r_A^2 - 2\mathbf{b}_i^T\mathbf{a}_i. \tag{3}$$

If $\mathbf{b}_i^T\mathbf{a}_i = 0$, i.e. if point $B_i$ lies on the $z$-axis, then Eq. 3 degenerates. That is to say, if, in addition, $\|\mathbf{b}_i\|^2 = \ell^2 - r_A^2$, then the IKP has an infinite number of solutions.

From the definition of articular coordinate $\theta_i$, we have that $\mathbf{a}_i = r_A\,[\cos\theta_i, \sin\theta_i, 0]^T$. Let also the components of vector $\mathbf{b}_i$ be $x_{B_i}$, $y_{B_i}$, and $z_{B_i}$. Then, Eq. 3 reduces to

$$\cos\theta_i\; x_{B_i} + \sin\theta_i\; y_{B_i} = \frac{\|\mathbf{b}_i\|^2 + r_A^2 - \ell^2}{2r_A} \equiv p_i. \tag{4}$$

In order to have a real solution to this equation, the following inequality should hold true:

$$x_{B_i}^2 + y_{B_i}^2 - p_i^2 \equiv \Gamma_i \geq 0. \tag{5}$$

Unless $\Gamma_i = 0$, there exist two real solutions to Eq. 4, determined uniquely from:

$$\sin\theta_i = \frac{p_i y_{B_i} + x_{B_i}\delta_i\sqrt{\Gamma_i}}{\rho_i} \equiv S_i, \tag{6}$$

$$\cos\theta_i = \frac{p_i x_{B_i} - y_{B_i}\delta_i\sqrt{\Gamma_i}}{\rho_i} \equiv C_i, \tag{7}$$

$$\theta_i = \mathrm{atan2}(S_i, C_i), \tag{8}$$

where $\theta_i \in [-\pi, \pi]$, $\delta_i = \pm 1$ is the *branch index*, and $\rho_i = x_{B_i}^2 + y_{B_i}^2$ is the squared length of the projection of vector $\mathbf{b}_i$ onto the $xy$ plane. The set of all branch indices will be referred to as *branch set*. As mentioned before, if $\rho_i = 0$, i.e., point $B_i$ lies on the $z$-axis, any $\theta_i$ is a solution to the IKP of chain $i$.

The organization of the rest of this paper is as follows. In Section 2, we describe geometrically the singularity surfaces of the *Rotobot* for a constant orientation of the mobile platform. Our task is simplified by taking advantage of the redundancy of the *Rotobot*. Important remarks are also made on the singularities of 6-DOF parallel mechanisms with pair-wise coincident

spherical joints and adjacent chains sharing a common track. In Section 3, we adapt and enhance the already-known methodology used for computing the constant-orientation workspace of the *Rotobot* by including the physical requirement of preserving the order of the *U*-joint centers along the track. Then in Section 4, we discuss on the elusive issue of branch sets which directly affects the workspace of the *Rotobot*. Finally, examples of the workspace and singularity surfaces of the *Rotobot* are shown in Section 5 and conclusions are made in the last Section 6.

## 2 SINGULARITY SURFACES

Having resolved the IKP we may now proceed to obtaining the velocity equations by differentiating Eq. 2 with respect to time:

$$\ell \mathbf{n}_i^T \left( \dot{\mathbf{c}} + \dot{\mathbf{R}} \mathbf{m}_i' - r_A \dot{\theta}_i \begin{bmatrix} -\sin\theta_i \\ \cos\theta_i \\ 0 \end{bmatrix} \right) = 0. \tag{9}$$

Expressing $\ell \mathbf{n}_i$ as

$$\ell \mathbf{n}_i = \begin{bmatrix} x_{Bi} - r_A \cos\theta_i \\ y_{Bi} - r_A \sin\theta_i \\ z_{Bi} \end{bmatrix}, \tag{10}$$

and using the fact that $\dot{\mathbf{R}} \mathbf{m}_i' = \dot{\mathbf{R}} \mathbf{R}^T \mathbf{m}_i = \boldsymbol{\omega} \times \mathbf{m}_i$, where $\boldsymbol{\omega}$ is the angular velocity of the mobile platform, and the fact that $\mathbf{n}_i^T (\boldsymbol{\omega} \times \mathbf{m}_i) = (\mathbf{m}_i \times \mathbf{n}_i)^T \boldsymbol{\omega}$, we obtain

$$\ell \left[ (\mathbf{m}_i \times \mathbf{n}_i)^T, \, \mathbf{n}_i^T \right] \begin{bmatrix} \boldsymbol{\omega} \\ \dot{\mathbf{c}} \end{bmatrix} = r_A (y_{Bi} \cos\theta_i - x_{Bi} \sin\theta_i) \dot{\theta}_i. \tag{11}$$

Finally, substituting $\sin\theta_i$ and $\cos\theta_i$ in the above equation with the expressions found in Eqs. 6 and 7, simplifying, and writing in matrix form gives us the final velocity equation:

$$\ell \begin{bmatrix} (\mathbf{m}_1 \times \mathbf{n}_1)^T & \mathbf{n}_1^T \\ \vdots & \vdots \\ (\mathbf{m}_6 \times \mathbf{n}_6)^T & \mathbf{n}_6^T \end{bmatrix} \boldsymbol{\xi} = -r_A \begin{bmatrix} \delta_1 \sqrt{\Gamma_1} & & 0 \\ & \ddots & \\ 0 & & \delta_6 \sqrt{\Gamma_6} \end{bmatrix} \dot{\boldsymbol{\theta}} \tag{12}$$

where $\boldsymbol{\xi} = [\boldsymbol{\omega}^T, \, \dot{\mathbf{c}}^T]^T$ is the *twist* of the mobile platform, and $\dot{\boldsymbol{\theta}} = [\dot{\theta_1}, \dot{\theta_2}, \ldots, \dot{\theta_6}]^T$ is the vector of active joint rates. We will denote the matrices multiplying the platform twist and the active joints rates with $\mathbf{Z}$ and $\boldsymbol{\Lambda}$, respectively. Thus, for every configuration, there is an equation

$$\mathbf{Z} \boldsymbol{\xi} = \boldsymbol{\Lambda} \dot{\boldsymbol{\theta}} \,, \tag{13}$$

which completely describes the velocity kinematics of the PM. These two matrices are usually referred to as Jacobian matrices.

Equation 13 completely describes the instantaneous kinematics of the *Rotobot* and hence can be used to fully describe and classify the singularity configurations of the mechanism. A general 6-*RUS* PM, as well as most parallel mechanisms, have two distinct types of singularities (Gosselin and Angeles, 1990). The first, or Type 1, occurs when matrix $\boldsymbol{\Lambda}$ is singular, while Type 2 corresponds to configurations where $\mathbf{Z}$ is singular.

The rows of matrix $\mathbf{Z}$ are the so-called *Plucker coordinates* of the lines along the distal links (Merlet, 1989). This fact was explored by Ebert-Uphoff et al. (2000) who studied geometrically the Type 2 singularity configurations for 6-DOF parallel mechanisms with three *S*-joints at the mobile platform. The authors classified the singularity configurations into several groups based on the relationship between the plane of the platform and three planes through the *S*-joints. Their approach can be applied directly to the *Rotobot* where the three planes will be the planes defined by the adjacent distal links. However, most of the groups for the particular design of the *Rotobot* represent very peculiar cases. Besides, the approach only gives a geometric insight and does not show how to obtain the singularity surfaces, which is our main task. Therefore, we will derive the expressions for the singularity surfaces by directly manipulating the Jacobian matrices. We strongly recommend the reader, however, to consider the above mentioned publication.

### 2.1 Type 1 Singularity Surfaces

From the above, it follows that a Type 1 singularity occurs only if $\Gamma_i = 0$. As used in the transition from Eq. 11 to Eq. 12

$$\mathbf{b}_i^T \mathbf{a}_i^{\perp} = -r_A \delta_i \sqrt{\Gamma_i} \tag{14}$$

where $\mathbf{a}_i^{\perp}$ is the vector obtained by rotating $\mathbf{a}_i$ about the $z$-axis by $90^\circ$. Hence, $\Gamma_i = 0$ when vector $\mathbf{b}_i$, or equivalently, vector $\mathbf{n}_i$, is normal to the tangent to the track at point $A_i$.

The complete set of positions of point $B_i$ that correspond to singularities of Type 1 forms a surface. From the description given in the previous paragraph, it can be easily seen that this surface is generated by sweeping a circle of radius $\ell$, the *generatrix*, about a circle of radius $r_A$, the *directrix* or, as we already call it, the track. The center of the generatrix lies on the track while the axis of symmetry of the generatrix is tangent to the track. Such a surface is, of course, a *right circular torus*.

This surface may have three distinctive shapes depending on the lengths of the proximal and distal links of the *RUS* chain. If the length of the distal link is smaller than the length of the proximal link, i.e., $\ell < r_A$, then the surface is a so-called *ring torus*, shaped like a doughnut. If $\ell = r_A$, the surface is called a *horn torus*, and if $\ell > r_A$, the surface is a *spindle torus*[*].

As we will see in Sections 3 and 4, the case $\ell \geq r_A$ makes the singularity and workspace analysis of the *Rotobot* much more intricate and ... intriguing. This is due to the existence of *self-intersection points* in the horn and spindle tori. Recalling Section 1.2, such points correspond to configurations at which the IKP of the serial chain has infinitely many solutions.

For a given constant orientation of the mobile platform, the Type 1 singularity surfaces for point $C$ may be obtained simply by translating the toroidal surfaces for each serial chain along the corresponding line $B_i C$. Naturally, there will be only three distinct Type 1 singularity surfaces for the *Rotobot*.

The volume enclosed by each of those surfaces is called the *vertex space*. Formally, vertex space $i$ is defined as the set of all

[*] `http://mathworld.wolfram.com/Torus.html`

possible positions that may be attained by point $C$ considering only the kinematic constraints of chain $i$ and keeping the mobile platform at a constant orientation. It is important to note that the *spindle torus* has a lemon-shaped cavity. Thus, any horizontal cross-section of any such vertex space will be an *annulus*, i.e., the area enclosed by two concentric circles.

Finally, let us point out an interesting fact related to the singularities of general 6-*RUS* PMs with pair-wise coincident *S*-joints and adjacent chains sharing a common track. At a Type 1 singularity, at least one pair of adjacent distal (and proximal) links is coincident. In other words, at least two rows of matrix $\mathbf{Z}$ will be identical. Hence, Type 1 singularities, in such mechanisms, are also Type 2 singularities. The only exception may be at the above mentioned self-intersection points. Namely, a pose, at which one of points $B_i$ is at a corresponding self-intersection point, corresponds to a Type 1 singularity. However, among the infinitely many possible placements for the corresponding two adjacent distal links, only some will lead to Type 2 singularities.

## 2.2 Type 2 Singularities

For a general 6-*RUS* PM, the IKP for each chain has two solutions, and hence, the IKP for the whole mechanism has 64 solutions. For a general 6-*RUS* (or other, e.g., 6-*PUS*) PM with pair-wise coincident *S*-joints and adjacent chains sharing a common track, however, there is only one solution, since in each adjacent pair of chains, each chain corresponds to one of the two solutions of the IKP for that pair. This important property determines the nature of the Type 2 singularities for such mechanisms.

Let us now look at the much simpler planar equivalent of the general 6-*RUS* PM, i.e., the planar 3-*RRR* PM. In a previous publication (Bonev and Gosselin, 2001), we showed that the singularity loci of 3-*RRR* PMs are dependent on the given branch set[†]. This is easy to understand by studying the determinant of the Jacobian matrix $\mathbf{Z}$. The latter contains the radical expressions $\delta_i\sqrt{\Gamma_i}$ and, hence, is dependent on the branch indices.

The same is true for the general 6-*RUS* PM. The problem with Type 2 singularities that are branch set dependent is that the expression defining them is not polynomial (it contains radicals) and hence the singularities are difficult to study and represent.

On the other hand, the advantage of such Type 2 singularities is that they may be modified without disassembling or reconfiguring the robot. Indeed, it is possible to change the branch index of one or more chains in order to change the Type 2 singularity loci and so be able to follow singularity-free trajectories that are otherwise impossible for a given branch set.

For a 6-*RUS* PM with pair-wise coincident *S*-joint centers and adjacent chains sharing a common track, it may be proven using a computer algebra system that the determinant of the Jacobian matrix $\mathbf{Z}$ is free of any radicals. In fact, for a constant orientation the determinant reduces to a polynomial of degree 18 in $x$, $y$, and $z$ (in the case $r_A = \ell$). This initially astonishing fact is actually quite obvious. Indeed, such a PM is kinematically the same for any branch set for which $\delta_j\delta_{j+1} = -1$, $j = 1,\ 3,\ 5$.

[†] `http://www.parallemic.org/Reviews/Review001.html`

### 2.2.1 The Rotobot as a redundant PM

Let us now focus on our *Rotobot* and determine its Type 2 singularity surfaces for a given orientation. Our task is quite simplified due to the fact that we need to specify only two Euler angles. Indeed, it is obvious that the Type 2 singularities remain the same when the mobile platform rotates about the $z$-axis since the configuration of the *Rotobot* remains unchanged. It can be shown, again using a computer algebra system, that the Type 2 singularities of the *Rotobot* can be represented by a polynomial of degree 5 in $x$, $y$, and $z$ (of degree 4 in $x$ and $y$). The polynomial is, however, still too big (some two pages) to represent in this paper.

In order to be able to describe in detail the derivation of the expression representing the Type 2 singularities we will limit ourselves to the case of the redundant *Rotobot*. (The procedure is almost the same as in the general case, though.) In other words, we will assume that the *Rotobot* is used with an axisymmetric tool along the mobile $z'$-axis, such as a milling cutter or a laser beam. Thus, there will be no need to orient the mobile platform about the mobile $z'$-axis and all required orientations of the mobile platform or, rather, all required directions of the axisymmetric tool may be realized by only one rotation. This rotation will be simply about the mobile $x'$ axis at an angle $\alpha$.

### 2.2.2 Derivation Procedure

We render our problem dimensionless and set $r_A = 1$. Once the Jacobian $\mathbf{Z}$ is expressed in the variables $x$, $y$, $z$, and the parameters $r_B$, $\ell$, $\alpha$, $\rho_j$, $\Gamma_j$, $\delta_j$, (recall that $\rho_j = \rho_{j+1}$, $\Gamma_j = \Gamma_{j+1}$, and $\delta_j = -\delta_{j+1}$) we follow the procedure described below (in this section $j = 1,\ 3,\ 5$).

**S1** Substitute the expressions $\delta_j\sqrt{\Gamma_j}$ with the parameters $\Delta_j$.

**S2** Obtain $\det\mathbf{Z}$. Its denominator is $128\rho_1^2\rho_3^2\rho_5^2$. Indeed, $\mathbf{Z}$ is not defined when point $B_i$ lies on the $z$-axis, i.e., when $\rho_j = 0$. Eliminating this case, we consider further only the numerator, $\mathcal{E}$. This numerator is a function of $x$, $y$, and $z$ that cannot be generally factored and contains the three radicals $\delta_j\sqrt{\Gamma_j}$ (actually $\Delta_j$) and the parameters $\rho_j$.

**S3** $\mathcal{E}$ can be factored to $\mathcal{E} = 3\sqrt{3}r_B^3\ell^8\Delta_1\Delta_3\Delta_5\mathcal{E}_1$, where $\mathcal{E}_1$ is an expression depending on $x$, $y$, $z$, $r_B$, $\ell$, $\alpha$, and $\rho_j$, and cannot be factored. Indeed, recall that the Type 1 singularities which are represented by $\Delta_j = 0$ are also Type 2 singularities. Hence, we are interested only in $\mathcal{E}_1$.

**S4** Substitute in $\mathcal{E}_1$ the expressions for $\rho_j = {x_B}_j^2 + {y_B}_j^2$:

$$\begin{aligned}\rho_1 &= (x - r_B\sqrt{3}/2)^2 + (y - \cos\alpha\, r_B/2)^2,\\ \rho_3 &= (x + r_B\sqrt{3}/2)^2 + (y - \cos\alpha\, r_B/2)^2,\\ \rho_5 &= x^2 + (y + \cos\alpha\, r_B)^2.\end{aligned}$$

**S5** Now, $\mathcal{E}_1$ depends only on $x$, $y$, $z$, $r_B$, $\ell$, and $\alpha$, and may be factored to $-96\sqrt{3}r_B\rho_1\rho_3\rho_5(z - \sin\alpha\, r_B/2)\mathcal{E}_2$, where $\rho_j$ are actually the above lefthand expressions. The singularity for $z = \sin\alpha\, r_B/2$ corresponds to the case where the horizontal side of the platform, $B_1B_3$, lies in the $xy$ plane.

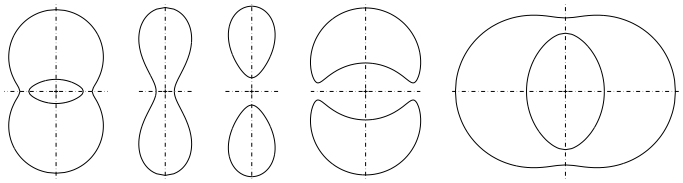

**Fig. 3 The types of shapes of the bicircular quartic.**

The singularity loci are in fact a bicircular quartic that is symmetric about the $x$-axis and the line $y = z\cot\alpha$. We perform a coordinate transformation $y = \overline{y} + z\cot\alpha$ and after factoring out a constant, we obtain the final equation for the Type 2 singularity loci for a given $z$:

$$\mathcal{Q} = (x^2 + \overline{y}^2)^2 + q_x x^2 + q_y \overline{y}^2 + q_0, \qquad (15)$$

where

$$\begin{aligned} q_x &= 2\ell^2 - 2 - r_B^2 + (2z^2 + 4zr_B\sin\alpha)/\sin^2\alpha, \\ q_y &= 2\ell^2 - 2 - r_B^2 - 2z^2/\sin^2\alpha, \\ q_0 &= (\ell^2\sin^2\alpha - 2zr_B\sin\alpha - \sin^2\alpha - z^2 - r_B^2\sin^2\alpha) \\ &\quad +(\ell^2\sin^2\alpha + 2zr_B\sin\alpha - \sin^2\alpha - z^2)/\sin^4\alpha. \end{aligned}$$

Once the equation of the quartic is known, it remains to plot it. As the equation is algebraic and not parametric, a method for discretizing it should be formulated. Such a method was devised by taking into account all possible shapes of the quartic (Fig. 3). The method is in fact a particular case of an algorithm created for the discretization of a general bicircular quartic needed for the computation of the constant-orientation workspace slices of a general 6-*RUS* PM (Bonev and Gosselin, 2000). The algorithm will be presented in the first author's Ph.D. thesis.

## 3 CONSTANT-ORIENTATION WORKSPACE

The methodology for computing the constant-orientation workspace of a general 6-*RUS* PM was described in detail in (Bonev and Gosselin, 2000). An exhaustive literature review on the subject was also presented. The workspace was visualized through its edges which were computed by analytical methods. The other alternative of representing the workspace through its horizontal cross-sections, will be detailed in the first author's thesis.

In this paper, however, we deal mainly with the *Rotobot* design, and the emphasis is on obtaining simple formulations for the singularities and workspace for a constant orientation that can be used for optimization purposes. In addition, our goal is to use the *Rotobot* design to show several new phenomena, rather than provide a practical tool for analyzing a particular *Rotobot*.

That is why, we choose to compute the constant-orientation workspace by horizontal slices. Firstly, the task is simpler, and secondly, we need cross-sections and not edges to be able to compute the volume of the workspace. The task of computing the workspace using a CAD system, as previously done (Bonev and Ryu, 1999), is overruled due to the difficulty in representing some of the geometrical objects (a quartic singularity surface and three Bohemian domes) and the necessity for some extra tests involving the solution of the IKP. We will not consider the mechanical limits of the *S* and *U* joints.

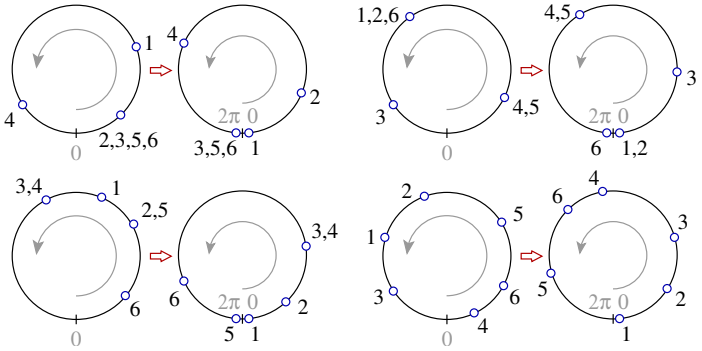


**Fig. 4 Four valid arrangements of the U-joint centers.**

### 3.1 Order of the U-Joints Along the Track

If we were able to construct the *Rotobot* in such a way that the *U*-joint centers $A_i$ along the track could change their order, then all that would have been necessary to do is to find the intersection between all three vertex spaces. The latter task amounts to being able to find the intersection of three annular regions (Gosselin, 1990). Unfortunately, most feasible designs would restrain the order of the *U*-joint centers along the track. In order to be able to easily model that physical constraint, we assume that *two or more* consecutive *U*-joint centers can coincide but not pass over. Thus, in our case points $A_1, A_2, \ldots, A_6$ should preserve their counter-clockwise order along the circular track.

For a given pose of the *Rotobot* we may solve the IKP and generally know the values for all six articular variables from Eq. (8). This is true if we choose to keep the branch index of each chain constant. However, as we will see in Section 4, two adjacent chains of the *Rotobot* may actually switch their branch indices simply by passing through a self-intersection singular point. Thus, by simply solving the IKP, we do not know immediately which of the two values in one of the three pairs of articular variables corresponds to one or the other chain in the corresponding adjacent pair of chains.

Even though the problem of verifying whether six points along a circle are in a given order seems quite easy, its solution is a challenging task due to the fact that the points may coincide. This task is even further complicated by the fact that we do not differentiate between the two points in each of the three pairs. The following procedure is proposed:

**S1** Form the ordered list $\boldsymbol{\vartheta} = \{\theta_1 + \pi, \ldots, \theta_6 + \pi\}$. Replace all elements that are equal to $2\pi$ by 0, so that $\boldsymbol{\vartheta} \in [0,\, 2\pi)$.

**S2** Reduce the numeric precision of all elements to, say, three digits after the decimal point. This is done to ensure that equal elements are indeed equal.

**S3** If $\vartheta_2 < \vartheta_1$, then interchange the values of $\vartheta_2$ and $\vartheta_1$. If $\vartheta_2 \geq \max\{\vartheta_3, \ldots, \vartheta_6\}$ and $\vartheta_1 \leq \min\{\vartheta_3, \ldots, \vartheta_6\}$, then interchange (maybe again) the values of $\vartheta_2$ and $\vartheta_1$. This is done to ensure that, if possible, point 2 is right after point 1 in a CCW direction.

**S4** Subtract $\vartheta_1$ from all elements of $\boldsymbol{\vartheta}$. Add $2\pi$ to all elements, that have become negative to make $\boldsymbol{\vartheta} \in [0,\, 2\pi)$. If any of or both $\vartheta_5$ and $\vartheta_6$ is/are equal to zero, then replace the zero with $2\pi$. If any of or both $\vartheta_3$ and $\vartheta_4$ is/are equal to zero and $\vartheta_2 \neq 0$, then replace the zero with $2\pi$ (Fig. 4).

**S5** Is $\vartheta_2 \leq \min\{\vartheta_3,\, \vartheta_4\}$ and $\max\{\vartheta_3,\, \vartheta_4\} \leq \min\{\vartheta_5,\, \vartheta_6\}$?

If the above test is positive, then the order of the six points is valid and we may obtain the branch indices for each chain. Particularly, $\delta_1 = -1$ if there was no interchange in the values of $\vartheta_1$ and $\vartheta_2$ in step 3; otherwise $\delta_1 = +1$. Similarly, $\delta_j = -1$ ($j = 3,\, 5$) if the $\vartheta_j < \vartheta_{j+1}$; otherwise $\delta_j = +1$. (If $\vartheta_j = \vartheta_{j+1}$ or $\vartheta_j = \vartheta_{j+1} \pm 2\pi$, the branch indices $\delta_j$ and $\delta_{j+1}$ are irrelevant.)

To perform the order test for a given branch only, steps 4 and 5 should be modified as follows (step 3 should be removed):

**S4'** Subtract $\vartheta_1$ from all elements of $\boldsymbol{\vartheta}$. Add $2\pi$ to those that became negative to make $\boldsymbol{\vartheta} \in [0,\, 2\pi)$. If $\vartheta_6 = 0$, set $\vartheta_6 = 2\pi$. If $\vartheta_i = 0$ and $\vartheta_{i-1} \neq 0$, set $\vartheta_i = 2\pi$ for $i = 3,\, 4,\, 5$.

**S5'** Is $\vartheta_2 \leq \vartheta_3 \leq \vartheta_4 \leq \vartheta_5 \leq \vartheta_6$?

### 3.2 Geometric Model for the U-Joint Interference

The vertex space boundary, as defined in Section 2.1, may be seen as the surface corresponding to all positions for the platform center, for a given constant orientation of the mobile platform, for which two *U*-joint centers are coincident. Inside the vertex space, the *U*-joint centers are not interfering.

A similar geometric model exists to describe the positions of the platform center for which two *neighboring U*-joint centers, i.e., $\{A_{j+1},\, A_k\}$, where $j = 1,\, 3,\, 5$ and $k = 3,\, 5,\, 1$ are coincident. Imagine, the mobile platform having a given orientation, with two coincident neighboring *U*-joint centers, $\{A_{j+1},\, A_k\}$. The platform center can move along a circle, $\mathcal{C}$, whose plane is normal to $B_jB_k$. The radius of this circle is equal to the distance from $A_k$ to line $B_jB_k$, i.e., $r_C = \sqrt{\ell^2 - 3r_B^2/4}$, and its center is at a point obtained by translating point $A_k$ along the constant vector $\mathbf{p}_k = -(\mathbf{m}_j + \mathbf{m}_k)/2$.

Now, notice that the above is true and remains the same for any position of the coinciding *U*-joint centers on the circular track. Hence, the complete set of positions of the platform center for which two neighboring centers are coincident is the *translation surface*, $\mathcal{B}_k$ obtained by sweeping circle $\mathcal{C}$, while its center moves on the track circle and the plane of the circle remains parallel to vector $B_jB_k$. Such a surface is a quartic surface and is called a *Bohemian dome* (Fig. 5). Its parametric equation is:

$$\mathcal{B}_k(u_k, v_k) = \mathbf{p}_k + \begin{bmatrix} r_C\cos\phi_k\cos u_k - r_C\sin\phi_k\cos\gamma_k\sin u_k + r_A\cos v_k \\ r_C\sin\phi_k\cos u_k + r_C\cos\phi_k\cos\gamma_k\sin u_k + r_A\sin v_k \\ r_C\sin\gamma_k\sin u_k \end{bmatrix} \quad (16)$$

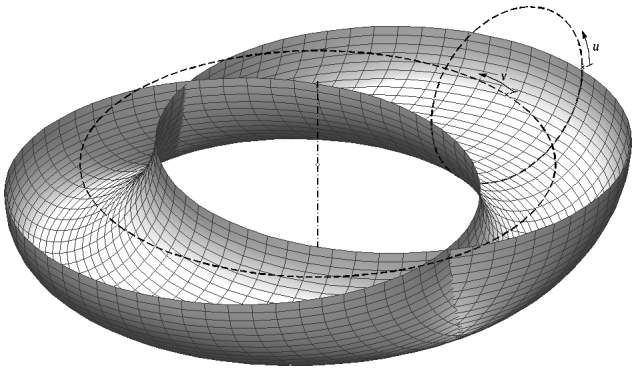


**Fig. 5 The lower half of a Bohemian dome.**

where the coordinate $u_k \in [0, 2\pi]$ defines the horizontal circular parallels and $v_k \in [0, 2\pi]$ defines the inclined circular parallels, and $\phi_k$ and $\gamma_k$ are respectively the azimuth and tilt angles defining vector $B_jB_k$ as:

$$\mathbf{m}_k - \mathbf{m}_j = \sqrt{3}r_B \begin{bmatrix} \sin\phi_k\sin\gamma_k \\ -\cos\phi_k\sin\gamma_k \\ \cos\gamma_k \end{bmatrix}. \quad (17)$$

Now, let us make the important observation that at the interior of the Bohemian dome $\mathcal{B}$, the two neighboring *U*-joint centers pass over and are, therefore, in interference. Hence, the platform center should always be at the exterior of that surface.

For a given value of $u_k$, the corresponding horizontal parallel is a circle of radius $r_A$ and center that can be directly obtained from Eq. 16. For a given height $z$, two values of $u_k$ can be generally found. Hence, for a given height $z$, there are generally two circles. And it is the area enclosed by those two circles, excluding the area inside both of them (if the circles are intersecting as in Fig. 16) that corresponds to *U*-joint interference and should be avoided. Note that for the heights $z_{k,min}$ and $z_{k,max}$ for which $u_k = \pm\pi/2$, there is only one circle, but it does not limit the workspace area in any way. In other words, for $z \leq z_{k,min}$ and $z \geq z_{k,max}$ there is no interference between the two *U*-joints.

Finally, let us study the relationship between the Bohemian dome surface for chains $j+1$ and $k$ and the vertex spaces corresponding to those two chains (actually to pairs $\{j,\, j+1\}$ and $\{k,\, k+1\}$). By definition, the Bohemian dome should be inside both vertex spaces. The parametric equation of vertex space $j$ is

$$\mathcal{V}_j(u_j, v_j) = \begin{bmatrix} \cos v_j(\ell\cos u_j + r_A) \\ \sin v_j(\ell\cos u_j + r_A) \\ \ell\sin u_j \end{bmatrix} - \mathbf{m}_j, \quad (18)$$

where $u_j \in [0, 2\pi]$ and $v_j \in [0, 2\pi]$.

Using the parametric equations for $\mathcal{V}_j$, $\mathcal{V}_k$, and $\mathcal{B}_k$, it can be shown that $\mathcal{B}_k$ is not simply inside both vertex spaces but is tangent to their boundaries. This amazing geometrical fact is demonstrated on Fig. 6, where the color interfusion (the smudges) on the MATLAB plot are due to the tangency between the surfaces. For a better representation, only the halves of the three entities are shown ($u \in [\pi, 2\pi]$).

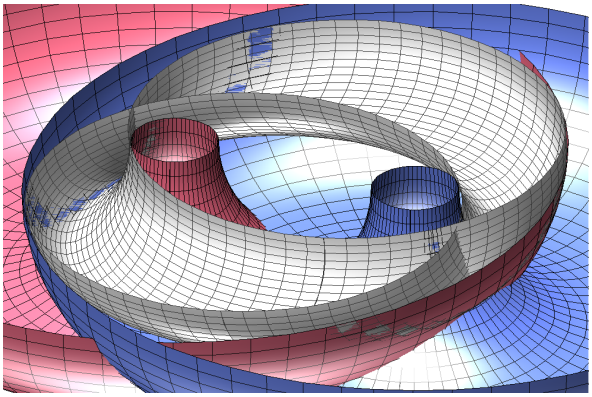

**Fig. 6 The lower halves of a Bohemian dome and the corresponding vertex spaces**

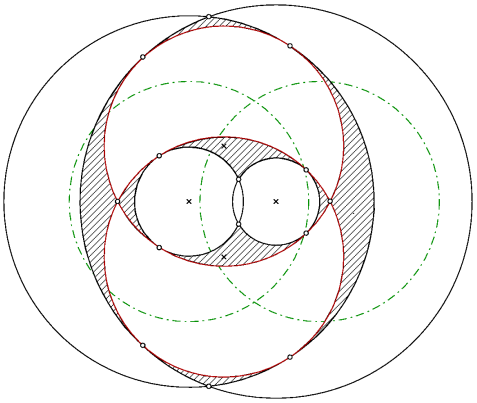

**Fig. 7 Horizontal cross-sections of a Bohemian dome and the corresponding vertex spaces**

An easier to understand way of proving the above fact is by using the algebraic expressions for the horizontal cross-sections of $\mathcal{V}_j$, $\mathcal{V}_k$, and $\mathcal{B}_k$. Unfortunately, even though these expressions can be found directly, they are too large to be included in this paper. An example of the cross-sections is given in Fig. 7. Basically, we have two pairs of concentric circles (from the vertex spaces) whose mean radius is $r_A$ (the radius of the dash-dotted circles), and two non-concentric circles of radius $r_A$ (from the Bohemian dome). Each of the two non-concentric circles is tangent to all four concentric circles. The hatched area is the area where the platform center can move without causing interference between the two neighboring *U*-joint centers $A_{j+1}$ and $A_k$.

### 3.3 Procedure for Computing the Workspace

We are finally ready to describe the computational procedure for computing the horizontal cross-sections of the constant-orientation workspace of the *Rotobot*.

For a given orientation, set the range $z \in (z_{min}, z_{max})$ for which all three vertex spaces exist and the distal links are always above the $xy$ plane, where $z_{max} = \ell - \max\{m_{1,z}, m_{3,z}, m_{5,z}\}$ and $z_{min} = -\min\{m_{1,z}, m_{3,z}, m_{5,z}\}$ ($m_{j,z}$ are the $z$ components of vectors $\mathbf{m}_j$). Start decrementing $z$ from $z_{max}$ down to $z_{min}$. To achieve a better visual result, it is not recommended to use a fixed interval step. We use, for example, the law $z = z_{max} \cos w$, where $w \in (\cos^{-1} z_{min},\, 0)$.

For each $z$, we compute the centers and radii of all three pairs of concentric circles (the cross-sections of the vertex spaces—they exist for sure) and the centers of the maximum three pairs of non-concentric circles (the cross-sections of the Bohemian domes—some or all may be missing). This data is stored in maximum six structure objects, each divided into two. Each of these maximum 6 times 2 objects correspond to a circle and contains fields for the geometrical data (center and radius), the intersection points (as values in the range $[0, 2\pi]$), and the pairs of intersection points that define the boundary arcs of the workspace cross-section.

For each two pairs of concentric circles, we compute and store the maximum four intersection points. If, for those two pairs, there exists a Bohemian dome, we compute and store the maximum two points of intersection between the two non-concentric circles. Finally, we calculate the eight points of tangency (recall Fig. 7) and store them in the appropriate fields.

Next, we take each of the maximum three pairs of non-concentric circles, and for each pair, we take each of the non corresponding vertex space concentric circles and each of the maximum two other pairs of non-concentric circles. For each pair of non-concentric circles and each pair of concentric or non-concentric circles, we compute the maximum 4 times 2 intersection points and store them in the appropriate fields.

At this stage, we have computed all possible intersection points between the maximum twelve circles. We then sort in ascending order all maximum twelve lists containing the values that define the intersection points. If the list of a circle has none or only one value, its contents is replaced with the pair $\{0,\, 2\pi\}$. Otherwise, we copy the smallest value at the end of the list. In this way, the consecutive values in each list define the consecutive arcs composing the circle.

Finally, we proceed to checking which of the resulting arcs are part of the workspace boundary. For each of the maximum twelve circles, start testing each arc. Find the coordinates of the middle point of each arc. Then, solve the IKP. If some $\Gamma_j$ ($j = 1,\, 3,\, 5$) is negative, then stop and start with the next arc. If all $\Gamma_j$ are non-negative, then perform the tricky test on the order of the *U*-joint centers (Section 3.1). If the test is negative, then stop and start with the next arc. Otherwise, put the values defining the arc in the third field of the structure object and repeat the procedure with the next arc until all arcs have been tested.

When all valid arcs have been identified, we may construct the workspace boundary array. Discretize each arc into a finite number of sequential points, as pairs of $\{x,\, y\}$ coordinates, and put them into the array. If using Matlab, add the {`NaN`, `NaN`} pair after each arc list. Note that we do not sort the arcs to obtain the boundary as an ordered list of closed contours, which is needed if we wish to compute the area of the workspace cross-section.

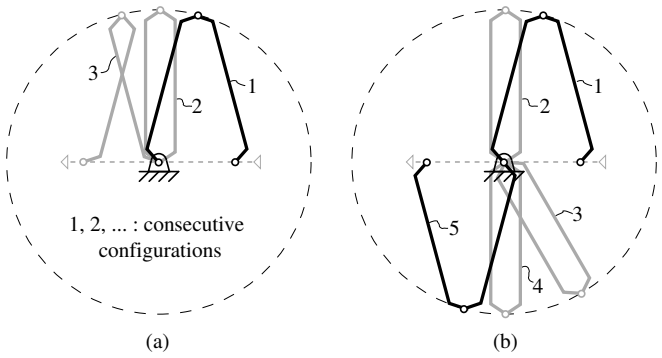


**Fig. 8 Passing through a self-intersection point by (a) changing or (b) keeping the branch index.**

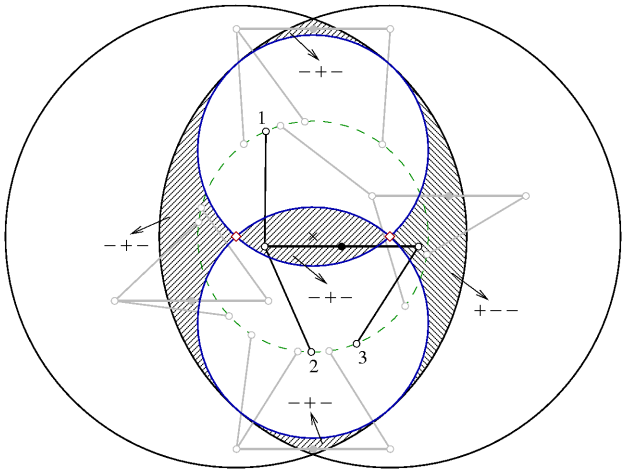


**Fig. 9 Division of the workspace of a 3-RRR planar PM according to its branch set.**

The list is now ready to be plotted. We may now discretize the bicircular quartic defining the Type 2 singularity loci (Section 2.2.2) and plot the parts that are inside the workspace.

**N.B.** For simplicity, we have considered that $C$ is the point of interest, i.e., the tool-tip. Obviously, this is not always the case. However, since the mobile platform has a constant orientation, we only need to offset all of the results presented in this paper if we are interested in another point of the mobile platform.

## 4 BRANCH SETS

Although, our task seems completed, we will go a step further and contemplate the important issue of branch set that probably remained unperceived.

The branch index of any *RUS* chain is determined by the initial assembly of the chain and may change only if the chain passes through a singularity. When $\ell < r_A$, the singularity surface for the *S*-joint center is a ring torus. Thus, there is only one sort of singularity that may occur in the chain. Namely, for any point at the surface, i.e., at the boundary of the vertex space, the two branches for the *RUS* chain coincide. Hence, the branch index of such a chain can be changed only when "bouncing off" of the vertex space boundary. Note, however, that for *Rotobot* it would be required that two adjacent *U*-joint centers interchange by passing over which is impossible. Therefore, the chains of a *Rotobot* with $\ell < r_A$ cannot change their branch indices. However, as we will see, this is not true in the case $\ell \geq r_A$.

Why do we bother about changing or keeping constant the branch index of a chain? Well, first of all, a robot controller should "know" how to solve the IKP for each serial chain. And second, the workspace of some parallel mechanisms depends on the given branch set—an important fact that is not widely known. Indeed, there only one parallel mechanism has been reported, a planar *PRRRP* one, with a controller that ingeniously uses inertia to switch between branch sets (Hesselbach et al., 2002).

There are two reasons, mainly practical, for keeping the branch index of a chain constant. Firstly, the mechanism would not be required to pass through a Type 1 singularity, which may be a problem depending on the adopted control scheme. Secondly, the distal link will be confined to only half a plane/space, with respect to the proximal link. Note that the angle between the proximal and distal links is already limited by the mechanical range of the connecting joint.

Now, recall that for an *RUS* chain with $\ell \geq r_A$, the serial chain singularity surface—a horn or spindle torus—has one or two self-intersection points representing a special sort of singularity. If the *S*-joint center passes through such a point along a path that lies completely inside the toroidal surface (except at that point) *with a continuous motion*, a change in the branch index occurs. This is easily illustrated by the identical situation of a planar *RRR* chain with equal proximal and distal links (Fig. 8). The figure illustrates clearly the practical meaning of a branch index change (see configuration 3 of Fig. 8a). It also suggests that while inertia may alow the transition through a branch index change, the transition keeping the branch index constant would certainly require an additional motor at the first *R*-joint. For a 3-*RRR* or 6-*RUS* general parallel mechanism, the only advantage of passing through one of these singularity points, with a branch index change, for some desired path may be the execution of a minimal *articular* trajectory.

For the *Rotobot* and some other designs, however, another advantage exists which is that new regions of the workspace might be attained. This point will be illustrated with a planar 3-*RRR* PM, shown in Fig. 9, whose base *R*-joints are all coincident, proximal and distal links are of the same length $\ell$, and two of the platform *R*-joints are coincident. For simplicity, we have not drawn the proximal links, but instead shown the circular track (the dashed circle) along which all three intermediate *R*-joints move. The initial assembly of the mechanism imposes that the three intermediate joints $(1,\ 2,\ 3)$ are arranged in a CCW order. The center of the mobile platform is represented by the dot symbol. For the zero orientation, we have drawn the two vertex spaces, which are the large circles of radius $2\ell$. Their centers,

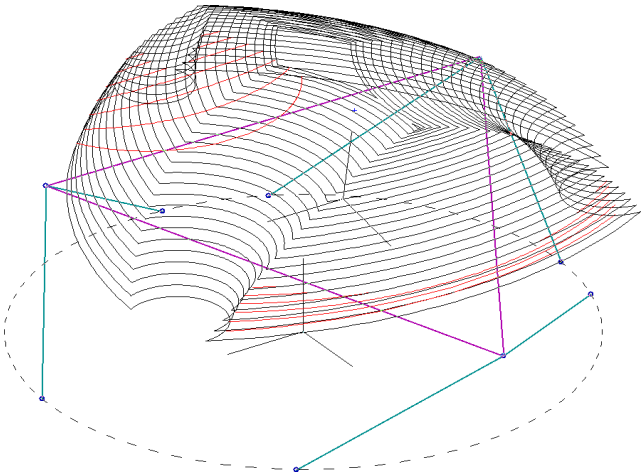

**Fig. 10 Constant-orientation workspace and singularity loci for a Rotobot design.**

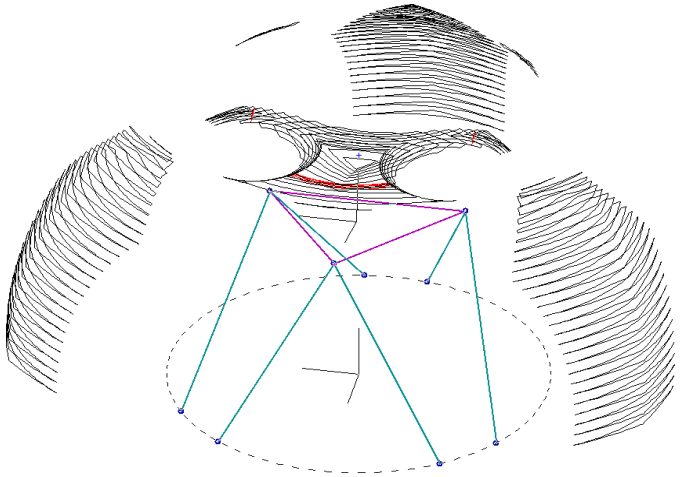

**Fig. 11 Constant-orientation workspace and singularity loci for a Rotobot design.**

represented by the two diamond symbols, correspond to the same self-intersection point singularities as in some 6-*RUS* chains.

Similarly to the Bohemian dome in the case of the *Rotobot* the set of positions that correspond to a change in the order of the intermediate joints is the interior of two circles of radius $\ell$ excluding the area inside both circles. Again, these two circles are tangent to and inside both vertex spaces. Hence, the constant-orientation workspace of the mechanism is the hatched zone.

Erroneously, some would wrap up the problem at this point. Careful examination, however, shows that the workspace is, in fact, divided into two different areas. The branch set corresponding to each of the five separate zones is shown and illustrated by a sample configuration of the mechanism. As it can be seen, the right-most segment corresponds to a switch in the branch indices of the adjacent chains 1 and 2. This change occurs when passing through the right self-intersection point.

Note that the constant-orientation workspace, and everything else, for a different orientation $\phi$ of the mobile platform will be exactly the same as that for $\phi = 0$ but rotated about the center of the base *R*-joints (marked with an "$\times$") at an angle $\phi$. Therefore, the complete 3D workspace will continue to be separated into 5 disconnected volumes, one of which will correspond to a different branch set.

Similarly, the workspace of the *Rotobot* is divided into segments that correspond to different branch sets. Regardless of whether those different segments will be explored via a branch set change or not, it is imperative to take this branch set phenomenon into account when describing the workspace of the *Rotobot*. This same phenomenon may occur for other parallel mechanisms with branch sets.

## 5 EXAMPLES

The proposed methodology was implemented in MATLAB 6, taking full advantage of its data structures and cell arrays. The computation time for the workspace is several seconds only. Computing and plotting the whole singularity curves, as well, doubles the computation time. If instead, only the segments of the singularity curves inside the workspace are plotted, the computation time builds up to a minute.

We present several examples for several different designs that illustrate the ideas developed in this paper. The first example, shown in Fig. 10, presents the constant-orientation workspace of the design that was chosen by Hexel for their commercially available prototype of the *Rotobot* ($r_A = r_B = 500$ mm, $\ell = 433$ mm). Their design requires a much more simplified workspace computation due to the fact that the distal links are shorter than the proximal links and the distance between two *S*-joint centers is greater than twice the length of the distal links. These mechanical limits ensure respectively a constant branch set and no *U*-joint interference. Even if the choice of the design was probably governed by the simplicity of the workspace computation, we should admit that the design seems to be quite optimal, with a "well-shaped" workspace that is almost singularity free. Figure 10 shows the horizontal cross-sections of the workspace boundary (in black) and singularity loci (in red) for the orientation defined by $\alpha = -10^\circ$. The *Rotobot* is also shown at the position $x = -140$ mm, $y = -60$ mm, and $z = 380$ mm. Note that for this design, as well as for the others to come, the tool-tip for which all computations are made (shown as a small blue "+") is selected at $z' = 200$ mm.

The second example, shown in Fig. 11, refers to a design for which $r_A = 500$ mm, $r_B = 300$ mm, and $\ell = 650$ mm. The orientation of the mobile platform is defined by $\alpha = 10^\circ$ and the *Rotobot* is shown at the pose for which its tool-tip is at $x = y = 0$ and $z = 720$ mm. The constant-orientation workspace at this orientation is divided into six volumes, of which only the upper-most central three correspond to the branch set $\delta_j = -1$, $\delta_{j+1} = +1$ ($j = 1, 3, 5$). Note that for this branch set, the corresponding workspace is centrally located, while for the other branch sets, the workspace volumes are far from the $z$-axis.

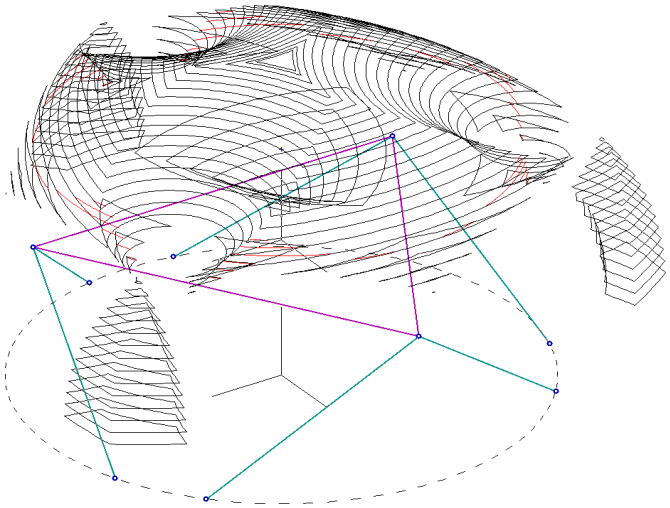

**Fig. 12 Constant-orientation workspace and singularity loci for a Rotobot design.**

The final example, shown in Fig. 12, refers to a design for which $r_A = 500$ mm, $r_B = 450$ mm, and $\ell = 500$ mm. The orientation of the mobile platform is defined by $\alpha = 0$ and the *Rotobot* is shown at the pose for which its tool-tip is at $x = y = 0$ and $z = 500$ mm. The constant-orientation workspace at this orientation is divided into four volumes, of which only the upper-most central one corresponds to the branch set $\delta_j = -1$, $\delta_{j+1} = +1$ ($j = 1, 3, 5$).

Based on these and many other examples, we conlude that the Type 2 singularity loci are scarce and close the the workspace boundary, and thus do not substantially limit the workspace. The optimization of the *Rotobot* can, therefore, ignore the Type 2 singularity loci and focus of the constant-orientation workspace only. As the edges of the workspace boundary cross-sections represent arcs of circles, the areas of these cross-sections can be computed exactly. By integration, the volume of the whole workspace may further be obtained.

## 6 CONCLUSION

Given the fact that the *Rotobot* design has been patented by Hexel Corporation, one might argue that they are the only one to profit from our research. In fact, the simplified design of their machine reduces even further their benefit. However, most of the ideas presented in this paper have a much broader significance. For example, we demonstrated that the singularities of general 6-*RUS* (and 6-*PUS*) parallel mechanisms with pair-wise coincident *S*-joints and adjacent chains sharing a common track do not depend on the branch set. Then we presented the solution of the non-trivial problem for testing the order of six points on a circle. We also modelled the interference of the adjacent *U*-joint centers by a Bohemian dome whose amazing properties were studied in detail. The Bohemian dome comes up in the analysis of other parallel chains as well. Then we studied the concept of branch set and showed how it may affect the workspace of a parallel mechanism. Finally, the geometric approach used in our paper is an example of how parallel mechanisms should be analyzed.

## 7 ACKNOWLEDGEMENTS

The authors would like to thank Mr. Tommy Geary for his work on the CAD model of the *Rotobot* (Fig. 1). The financial support of the Canada Research Chair Programme and NSERC is also acknowledged.

## REFERENCES

Bonev, I.A., and Ryu, J., 1999, "Workspace Analysis of 6-PRRS Parallel Manipulators Based on the Vertex Space Concept," *Proceedings of the 1999 ASME Design Engineering Technical Conferences*, Las Vegas, NV, USA, DETC99/DAC-8647.

Bonev, I.A., and Gosselin, C.M., 2000, "A Geometric Algorithm for the Computation of the Constant-Orientation Workspace of 6-RUS Parallel Manipulators," *Proceedings of the 2000 ASME Design Engineering Technical Conferences*, Baltimore, MD, USA, DETC00/MECH-14106.

Bonev, I.A., and Gosselin, C.M., 2001, "Singularity Loci of Planar Parallel Manipulators with Revolute Joints," *2nd Workshop on Computational Kinematics*, Seoul, Korea, pp. 291-299.

Chi, Y.L., 1999, *Systems and Methods Employing a Rotary Track for Machining and Manufacturing*, WIPO Patent No. WO 99/38646.

Gosselin, C. M., 1990, "Determination of the Workspace of 6-DOF Parallel Manipulators," *ASME Journal of Mechanical Design*, Vol. 112, September, pp. 331–336.

Gosselin, C.M., and Angeles, J., 1990, "Singularity Analysis of Closed-Loop Kinematic Manipulators," *IEEE Transactions on Robotics and Automation*, Vol. 6, No. 3, June, pp. 281–290.

Hesselback, J., Helm, M.B., and Soetebier, S., 2002, "Workspace-Optimized Parallel Robot for Placing Tasks," *Proceedings of the 2002 Parallel Kinematics Seminar*, Chemnitz, Germany, April 23-25, pp. 697–714.

Ebert-Uphoff, I., Lee, J.-K., and Lipkin, H., 2000, "Characteristic Tetrahedron of Wrench Singularities for Parallel Manipulators with Three Legs," *Proceedings of a Symposium Commemorating the Legacy, Works, and Life of Sir Robert Stawel Ball*, Trinity College, Cambridge, UK.

Merlet, J.-P., 1989, "Singular Configurations of Parallel Manipulators and Grassmann Geometry," International Journal of Robotics Research, Vol. 8, No. 5, pp. 45–56.

Merlet, J.-P., 1994, "Détermination de l'espace de travail d'un robot parallèle pour une orientation constante," *Mechanism and Machine Theory*, Vol. 29, No. 8, pp. 1099–1113.